J. Comput. Appl. Res. Mech. Eng. Vol. 10. No. 2, pp. 525-537, 2021 *DOI: 10.22061/jcarme.2019.4411.1541*

SRTTU

Journal of Computational and Applied Research in Mechanical Engineering

jcarme.sru.ac.ir

JCARME

ISSN: 2228-7922

Research paper

Effect of axial groove location, length, and width ratio on bearing properties and stability

Vijay Kumar Dwivedi[a*] and Pooja Pathak[b]

[a]*Department of Mechanical Engineering, GLA University, Mathura (U.P), 201406, India*
[b]*Department of Mathematics, GLA University, Mathura (U.P), 201406, India*

Article info:

Article history:

Received: 29/11/2018
Accepted: 10/06/2019
Revised: 13/06/2019
Online: 15/06/2019

Keywords:

Axial groove,
Damping coefficient,
Stiffness coefficient,
Stability.

[*]Corresponding author:
nain.pawan2@gmail.com

Abstract

There are many industrial applications of axially grooved journal bearing, especially in turbo- machinery. Stability is a very big issue for researchers, in high speed rotating machines. The axial groove journal bearing has a capacity to reduce the vibration and the ability to resolve the heating problems as well as stability at a higher speed. Dynamic performance parameters and stability of axial grooved hybrid journal bearings depend on the dimensions and orientations of the groove to a great extent at higher speeds. In this work, a FORTRAN program is used to solve Reynolds governing equation. The bearing performance characteristics are simulated for the various dimensions and orientation of the groove. Non-linear journal center trajectories are drawn for different Reynolds numbers for stability analysis. It is found that the smaller groove length results in lower bearing capacity, whereas smaller groove width yields higher bearing capacity, and the turbulence decreases the stability. The groove location also strongly affects most performance parameters. The optimum location of the groove axis is obtained between 60° to 90° to the load line.

1. Introduction

Turbo-machinery with high load and high journal speed are widely used in hybrid bearings. The lubricant is often delivered through one or two grooves at a prescribed pressure from a supply hole at the inlet. Groove dimensions and their number have a significant effect on bearing performance. These grooves are cut into inner surface of the bearing. Depending on the application, the groove configuration can be axial, circumferential, and spiral. Usually, the groove is located at 90 on the load line, upstream of the minimum film thickness position.

O' Donoghue and Rowe [1, 2] developed an externally pressurized bearing design method based on pad load and flow coefficients that depend only on the geometric shape and proportions of the bearing and are independent of the control device used. They also proposed the exact procedure together with the Reynolds equation's computer solution for a finite

hydrostatic multirecess bearing using a finite difference method.

Koshal et al. [3, 4] also analyzed the effect of the a/L ratio on load-bearing capacity. They concluded that the load-bearing capacity increases with an increase in power ratio (K) for same a/L ratio. Andres and Szeri [5] presented the analytical solution for flow between eccentric rotating cylinders. Mortonet et al. [6] presented grooves' effect on rotating system stability and response. They found that grooved bearing modifies the locus of the journal by increasing the angle of attitude and also changes the boundary of cavitation at low ratios of excentricity, i.e., high speeds. Gethin and Deihi [7] used the finite element method to study the effect of loading direction on the performance of a twin axial groove bearing. They concluded that when the grooves are orthogonal to the load line, the load-carrying capacity is optimal. Sinhasan and Chadrawat [8] showed bearing properties for many deformation coefficient values and Reynolds number of two axial groove journal bearings operating in laminar and superlaminar flow regimes. Pai and Mazumdar [9] discussed the stability properties of submerged, unidirectional plain journal bearings under constant and variable rotating loads. A computer program for the analysis of journal bearing with boundary conditions was developed with the help of McCormick et al. [10]. Claro and Mirinda [11] studied the journal bearing characteristics by considering the lubricant supply conditions. Mishra and Kumar [12] presented the effects of geometric change on stability of hydrodynamic journal bearing due to wear. They concluded that the stability decreases due to wear of journal or bearing.

Mishra and Kumar [13] also analyzed the steady-state behavior of non-circular worn journal bearing. Martin [14] analyzed the flow of oil for plane loaded journal bearing. KaKoty and Mazumdar [15] studied the effect of fluid inertia on stability of oil journal bearings. They attempted to evaluate the mass parameter (a measure of stability) besides finding out steady-state characteristics of finite journal bearings considering the effect of inertia. Jerry and Su [16] investigated the rotation effect of the hybrid bearing. Costa et al. [17] investigated that one groove (located at load line) bearing has better performance. They also commented that twin groove journal bearing is widely used, especially when the shaft is expected to assume both directions of rotation. Majumdar et al. [18] obtained steady-state and dynamic characteristics, including whirl instability of water-lubricated journal bearing having three axial grooves theoretically. Desai et al. [19] carried out an analysis of pressure distribution of hydrodynamic journal bearings with different groove configurations. They suggested the use of a circumferential groove at the center of the bearing, with an oil supply hole located opposite the load-bearing zone. Brito et al. [20, 21] investigated experimentally the effect of temperature, pressure, and load applied on the performance of a journal bearing. They concluded that the increment in feeding pressure increases oil flow rate, reduces oil temperature, and increasesslightlythe angle of attitude and theminimum film thickness. Roy and Laha [22] investigated the steady-state and dynamic characteristics of axial groove journal bearing.Navthar and Halegowda [23] presented a method to determine the synchronous whirl, i.e., thestability of hydrodynamic journal bearings by using dynamic characteristics such as stiffness coefficients. Mehta et al. [24] further extended their work by using a couple of stress lubricants for the stability of two-lobe hydrodynamic bearing.Kini et al. [25] investigated the effect of groove location on the dynamic characteristics of multiple axial groove water-lubricated journal bearing. They obtained the stability characteristics of water-lubricated journal bearing having three axial grooves theoretically and obtained stiffness and damping coefficient for various bearing number and eccentricity ratio.Brito et al. [26] has compared the performance of journal bearing having single as well as twin axial groove journal bearing. Roy and Kakoty [27] presented the various arrangements of grooving location of two groove oil journal bearing for optimum performance.Dwivedi et al. [28-30] studied the effect of flow regime and recess shape on the static-dynamic performance of the hydrostatic andhydrodynamic bearing. They also carried the stability analysis of the journal bearing in different flow regimes.Brito et al. [31] presented a thermohydrodynamic (THD) model for

performance enhancement and friction reduction analysis of journal bearings with realistic feed condition. Dwivedi et al. [32] has analyzed the stability of journal bearing having twin axial grooves. Sharma and Awasthi [33] theoretically investigated the effect of transient wear on the performance of the hydrodynamic bearing. They concluded that effect of wear on all static and dynamic parameters increase with an increase in eccentricity ratio.Wang et al. [34] discussed the effect of geometry parameters on the load capacity andfriction coefficient of the bearing. They concluded that bearing load capacity is reduced by the concave spherical texture, but enhanced by the convex texture, whereas the surface textures have a very slight effect on the friction coefficient.

2. Theoretical model/analysis

A theoretical model was developed for the analysis of static and dynamic characteristics of two groove journal bearing. Fig. 1 shows the journal bearing configuration. Figs. 2 and 3 show the coordinate system of unwrapped bearing with fluid domain in 2-D and 3-D, respectively, considering very small fluid film thickness. α_1 and α_2, as shown in Figs. 2 and 3, represent positive fluid film pressure, whereas the location of the centerline of the grooves represent by α_{1g} and α_{2g}, respectively.

2.1. Flow field equation

Constatantinescu [35] presented a linearized turbulence theory, which governs the flow of lubricating oil in the clearance space between journal and bearing surface. He gave a dimensionless Reynolds equation given in Eq. (1).

$$\frac{\partial}{\partial\alpha}\left[\frac{\bar{h}^3}{\bar{\mu}\bar{K}_\alpha}\frac{\partial\bar{p}}{\partial\alpha}\right]+\frac{\partial}{\partial\beta}\left[\frac{\bar{h}^3}{\bar{\mu}\bar{K}_\beta}\frac{\partial\bar{p}}{\partial\beta}\right]=\frac{1}{2}\bar{\Omega}\left(\bar{X}_j\sin\alpha-\bar{Z}_j\cos\alpha\right)-\dot{\bar{X}}_j\cos\alpha-\dot{\bar{Z}}_j\sin\alpha \quad (1)$$

The dimensionless thickness of fluid film ($\bar{h}$) is given by:

$$\bar{h}=1-\bar{X}_j\cos\alpha-\bar{Z}_j\sin\alpha \quad (2)$$

2.1.1. Approximation of short bearing

Bearing is infinitely short and is assumed in short bearing approximation concept so that pressure gradient is very less in the circumferential direction, as compared to axial direction, i.e.:

$$\frac{\partial p}{\partial\alpha}\ll\frac{\partial p}{\partial\beta}$$

The Reynolds Equation reduces to;

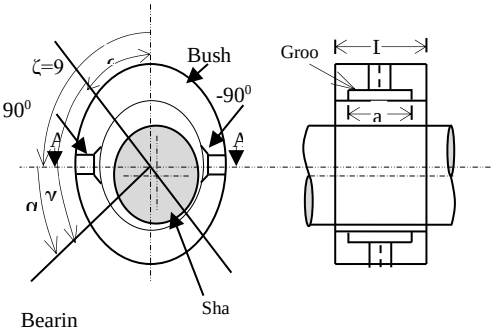

Fig. 1. Journal bearing configuration.

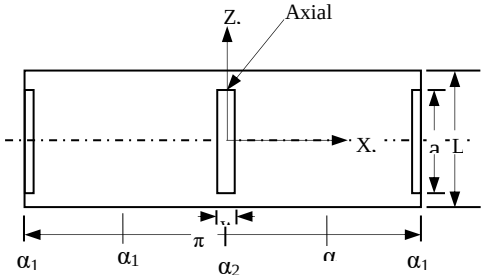

Fig. 2. Coordinate system of unwrapped bearing with fluid domain.

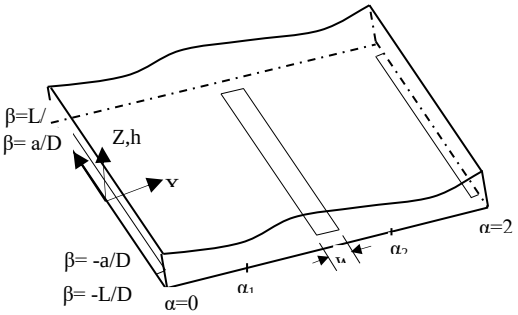

Fig. 3. Three dimensional view of fluid film between journal and bearing.

$$\frac{\partial}{\partial\beta}\left[\frac{\bar{h}^3}{\bar{\mu}\bar{K}_\beta}\frac{\partial\bar{p}}{\partial\beta}\right] = f(\alpha) \quad (3)$$

where $f(\alpha) = \frac{1}{2}\bar{\Omega}\left(\bar{X}_j \sin\alpha - \bar{Z}_j \cos\alpha\right) - \dot{\bar{X}}_j \cos\alpha - \dot{\bar{Z}}_j \sin\alpha$ (4)

Eq. (3) is solved using boundary conditions as discussed in Section 2.2.

2.2. Boundary conditions (B.C.)

The B.C. used for the current work are given below:

(i) $\frac{\partial\bar{p}}{\partial\beta} = 0$ at $\beta = 0$ (ii) $\bar{p} = 0$ at $\beta = \pm\frac{L}{D} = \pm\lambda$ (5a)

(iii) $\bar{p} = 0$ at $\left(\left(-\frac{a}{D} < \beta < \frac{a}{D}\right)\right.$ and $\left.\left((\alpha_{1g} - \frac{w}{D}) < \alpha < (\alpha_{1g} + \frac{w}{D})\right)\right)$ (5b)

(iv) $\bar{p} = 0$ at $\left(\left(-\frac{a}{D} < \beta < \frac{a}{D}\right)\right.$ and $\left.\left((\alpha_{2g} - \frac{w}{D}) < \alpha < (\alpha_{2g} + \frac{w}{D})\right)\right)$ (5c)

where α_{1g} and α_{2g} are the center lines of the angular position of grooves in radian.
By integrating Eq. (3) w.r.t. β and using B.C., Eq. (5) pressure distribution around the journal is obtained as:

$$\bar{p}(\alpha,\beta) = \left(\frac{\bar{\mu}\bar{K}_\beta}{\bar{h}^3}\right)\left(\frac{1}{2}f(\alpha)(\beta^2 - \lambda^2)\right) \quad (6)$$

2.3. Load bearing capacity

Journal bearing load carrying capacity is calculated by double integrating the pressure over the positive pressure zone in the axial and circumferential direction. Bearing capacity in X-direction (i.e. circumferential) is represented as:

$$\bar{F}_X = -\int_{-\lambda}^{\lambda}\int_{\alpha_1}^{\alpha_2} \bar{p}.\cos\alpha\, d\alpha.\, d\beta \quad (7)$$

and similarly bearing capacity in Z-direction (i.e. radial) is represented as:

$$\bar{F}_Z = -\int_{-\lambda}^{\lambda}\int_{\alpha_1}^{\alpha_2} \bar{p}.\sin\alpha\, d\alpha.\, d\beta \quad (8)$$

By using Gauss-Legendre integration method Eqs. (7 and 8) are solved numerically over the positive pressure zone.

2.4. Computation of fluid film stiffness and damping co- efficient

Fluid film stiffness and damping coefficients were obtained numerically by derivatives of fluid film force with respect to journal center and journal velocity component in axial and circumferential direction, respectively.

3. Computational procedures/ numerical model

Lubricant flow governing equation between bearing and journal (i.e., Reynolds equation) was modified to study the different flow regimes (laminar, transition, and turbulent flows), by including turbulence coefficients $\bar{K}_X$ and $\bar{K}_Y$. In this study, TheReynolds equationwas solved by using short bearing approximation. The closed-form pressure expression was obtained by integrating twice the Reynolds equation and using boundary conditions (as mentioned in Section 2.2), i.e., the bearing pressure at the mid-plane was maximum and the pressure at the end of the bearing was zero. Only a positive pressure zone was taken during the pressure calculation. Pressures below atmospheric and entire groove were not considered.

4. Results and discussion

Pressure profile, load-bearing capacity, fluid film stiffness coefficients, and damping coefficients were calculated with the help of analysis and solution algorithm. Developed numerical model (computer program) calculated all bearing performance parameters by taking length-diameter ratio (L/D) as 0.5 and 0.25, with assumptions such as parallel bearing and journal axes, and clearance ratio of 0.001 (C/R = 0.001).

4.1. Validation of results

The validity of the analysis, solution algorithms, and the developed computer model were established by comparing the dimensionless load capacity for different groove locations obtained from the present short bearing approximation with the results available in the literature of Gethin and Deihi [7], Kumar and Mishra [13], Brito et al. [31], and Sharma and Awasthi [33].

In Fig. 4(a), the comparison of nondimensionalized load-bearing capacity with different groove locations is shown for laminar flow conditions with an aspect ratio of 0.50, clearance ratio of 0.004, and eccentricity of 0.7 between the authors work and available results of Gethin and Deihi [7]. In Fig. 4(b), the comparison of circumferential pressure with angular location from X-axis is shown for **an** aspect ratio of 0.50, clearance ratio of 0.001, and speed of 2000 and 4000 rpm between the authors work and available results of Brito et al. [31].

Fig. 4(c) graphically explains the variations of eccentricity ratio (e) and attitude angle with Sommerfeld number (Sn) at Reynolds number=5000, an aspect ratio of 1.0, wear depth of 0.0, and clearance ratio of 0.001. Results compare well within the acceptable variations due to different methodologies of the solution with the results of Sharma and Awasthi [33] and Kumar and Mishra [13].

4.2. Effect of the a/L on dimensionless direct stiffness coefficient

The variation of direct stiffness coefficients ($\overline{K}_{XX}, \overline{K}_{XZ}, \overline{K}_{ZX}, \overline{K}_{ZZ}$) with a/L are shown in Figs. 5-8. It is seen from Figs. 5 and 6 that direct stiffness coefficients in X and Z directions reduce linearly with increment in a/L. The magnitude of the cross-coupled damping coefficient Z-X directions is negative over the entire range of a/L.

It is seen from Fig. 7 that $\overline{K}_{ZX}$ first reduces with increment in a/L then stabilizes at a fixed value. The minimum value of $\overline{K}_{ZX}$ = 4.13. Fig. 8 shows direct stiffness in Z-direction. As Fig. 8 shows, a similar trend is found to the $\overline{K}_{ZX}$, i.e., first, it reduces before settling to a fixed value.

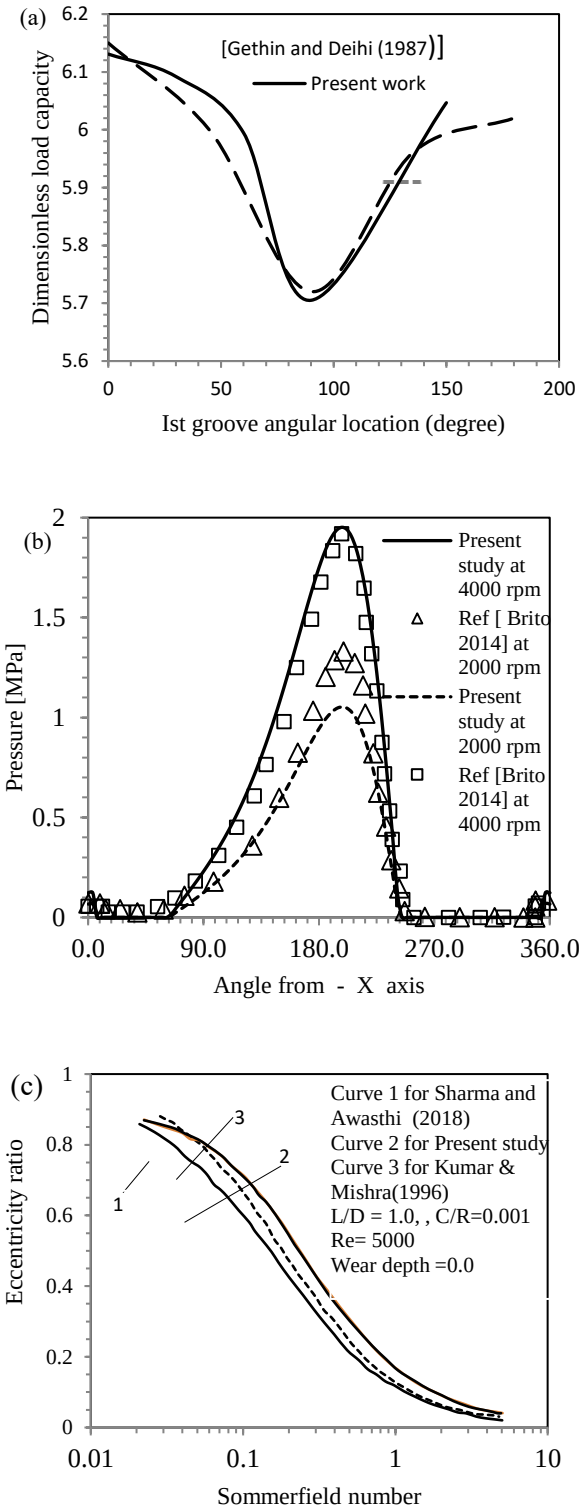

Fig. 4. (a) Nondimensionalized load capacity Vs groove location, (b) Comparison of pressure profile of the bearing between present analysis and experimental data of Brito et al. [31], (c) Eccentricity ratio Vs Sn for aspect ratio = 0.50 for variation of Re.

4.3. Effect of the a/L on direct and cross coupled damping coefficient

Figs. 9-11 represents the stiffness coefficients ($\bar{C}_{XX}, \bar{C}_{XZ}, \bar{C}_{ZZ}$), which are shown for variation in a/Lwith fixed w/D ratio of 0.02. It is observed from Fig. 9 that the direct damping coefficients in the X-direction, $\bar{C}_{XX}$, increases with an increase in a/L before settling to a fixed value. Whereas, direct damping coefficient in the Z-direction, $\bar{C}_{ZZ}$, as shown in Fig. 11, initially decreases up to a/L= 0.17, then increases before settling to a fixed value with an increase in a/L. Damping coefficients in the Z-X direction reduces with increment in a/L before settling. From Figs. 9-11, it is concluded that the a/L ratio has a significant effect on damping coefficients up to a/L of 0.4. Thereafter, it does not affect the damping coefficients.

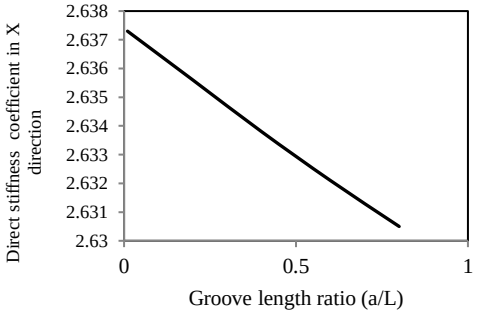

Fig. 5. Effect of a/L on, $\bar{K}_{XX}$.

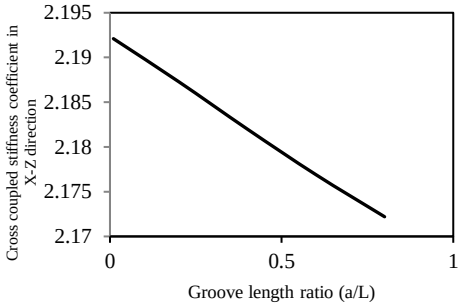

Fig. 6. Effect of a/L on $\bar{K}_{XZ}$.

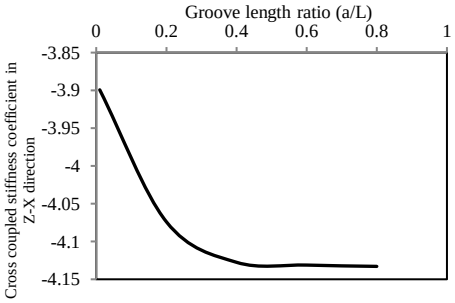

Fig. 7. Effect of a/L on $\bar{K}_{ZX}$.

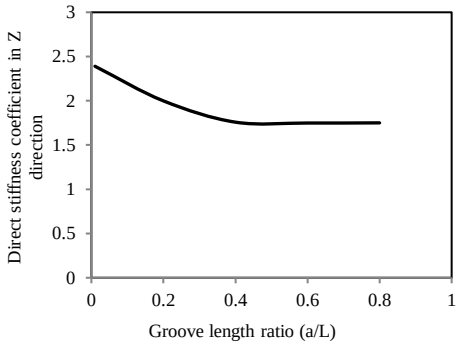

Fig. 8. Effect of a/L on $\bar{K}_{ZZ}$.

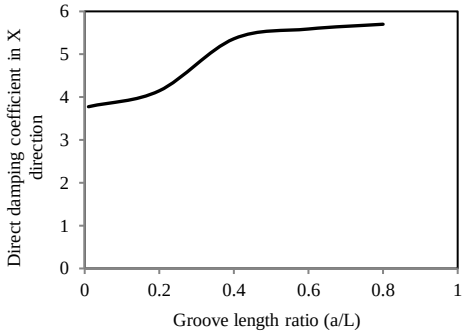

Fig. 9. Effect of a/L on $\bar{C}_{XX}$.

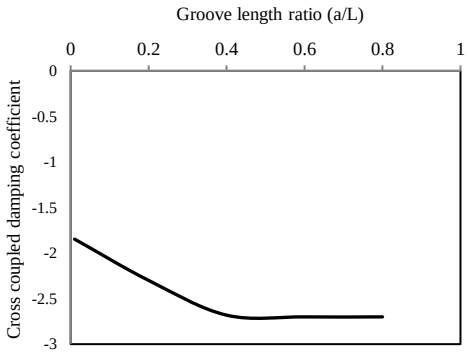

Fig. 10. Effect of a/L on, $\bar{C}_{XZ}$.

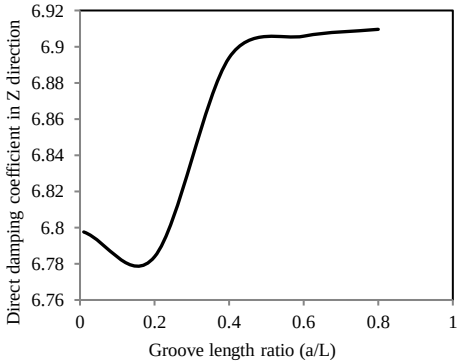

Fig. 11. Effect of a/L on $\bar{C}_{ZZ}$.

4.4. Effect of the w/D on stiffness coefficient

Figs. 12-15 show the effect of the w/D on stiffness coefficient. It is seen from Fig. 12. that $\bar{K}_{XX}$ is fixed up to w/D = 0.10 then reduces with increment in w/D. Fig. 13 shows that $\bar{K}_{XZ}$ reduces with increment in w/D before stabilizing to a fixed value. The lowest value of $\bar{K}_{XZ}$ = 1.43. It is seen from Fig. 14. that $\bar{K}_{ZX}$ increases with a reduction in w/D. Fig. 15 shows that $\bar{K}_{ZZ}$ is fixed initially up to w/D = 0.10 then increases with increment in w/D.

4.5. Effect of the w/D on damping coefficient

Figs. 16-18 show the effect of the w/D on direct and cross-controlled stiffness coefficient ($\bar{C}_{XX}, \bar{C}_{XZ}, \bar{C}_{ZZ}$). Direct damping coefficient in X direction $\bar{C}_{XX}$ reduces with increment in w/D before settling to a certain point. The rate of decrement is highest between w/D = 0.1 and w/D = 0.2. The direct damping coefficient in Z direction $\bar{C}_{ZZ}$ reduces with increment in w/D up to 0.2. Thereafter, it starts increasing with the increase in the w/D ratio. The rate of decrement is maximum between the w/D ratio of 0.1 to 0.2, similar to the trend for $\bar{C}_{XX}$.

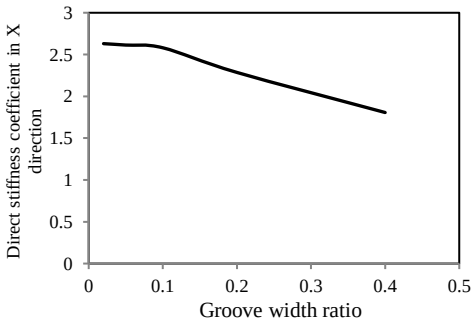

Fig. 12. Effect of w/D on $\bar{K}_{XX}$.

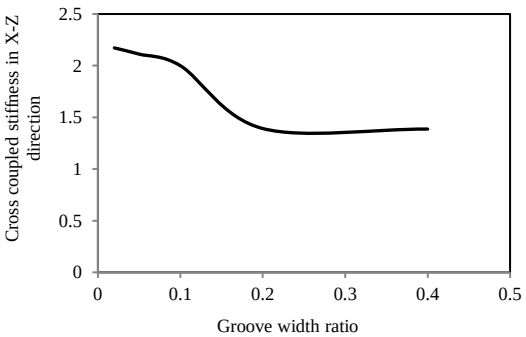

Fig. 13. Effect of w/D on $\bar{K}_{XZ}$.

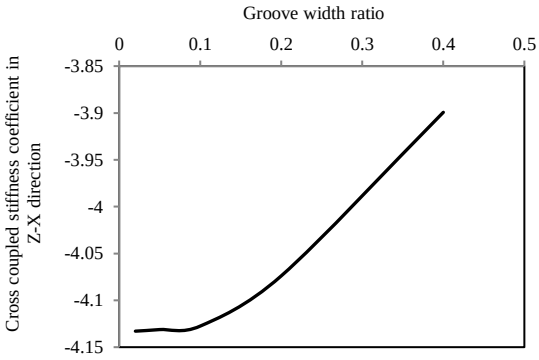

Fig. 14. Effect of w/D on $\bar{K}_{ZX}$.

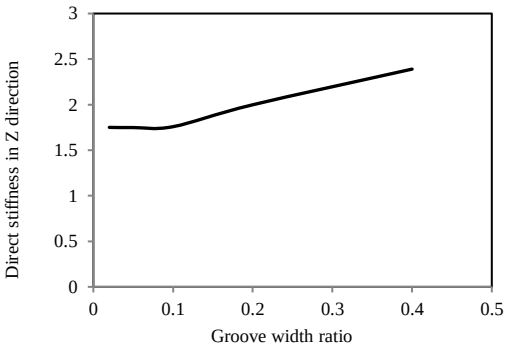

Fig. 15. Effect of w/D on $\bar{K}_{ZZ}$

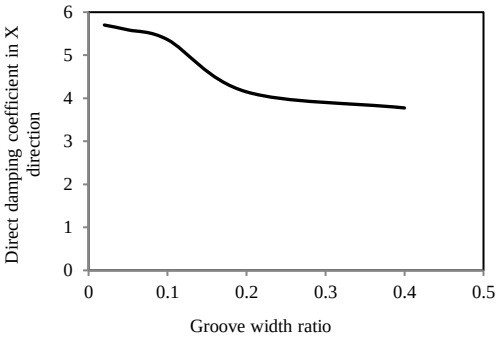

Fig. 16. Effect of w/D on $\bar{C}_{XX}$.

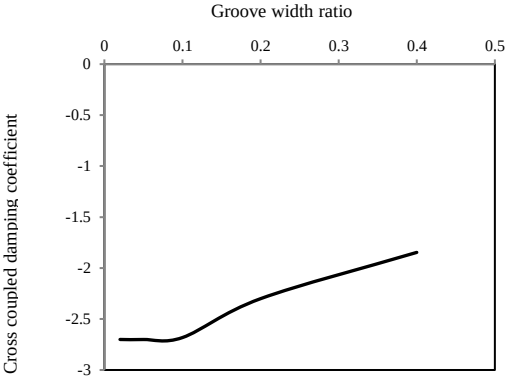

Fig. 17. Effect of w/D on ($\bar{C}_{XZ}$= $\bar{C}_{ZX}$).

The value of cross $\bar{C}_{XZ}$ and $\bar{C}_{ZX}$ are not positive for all groove width ratio. It is seen from Fig. 17 that the $\bar{C}_{XZ}$ is initially fixed up to w/D = 0.1 after that, $\bar{C}_{XZ}$ increases with increment with w/D.

4.6. Effect of radial position of the axial grooves on stiffness coefficient

Figs. 19-22 shows the variation of $\bar{K}_{XX}$, $\bar{K}_{XZ}$, $\bar{K}_{ZX}$ and, $\bar{K}_{ZZ}$ with the radial position of the Ist groove. The position of the Ist groove is 180^0 earlier than the IInd groove. Fig. 23 shows that the variation of $\bar{K}_{XX}$ increment with increment in radial position of Ist groove up to α_{1g} equal to 90^0. The best value of Ist groove radial position α_{1g}= 90^0 is seen at which direct stiffness coefficient is highest, i.e., $\bar{K}_{XX} = 2.829$. The indirect stiffness coefficient $\bar{K}_{XZ}$ is shown in Fig. 20. The similar behavior has been seen in the case of $\bar{K}_{XX}$ with Sn. The best value of indirect stiffness $\bar{K}_{XZ}$ is 2.349 at 90^0 of Ist groove angular position.

The value of indirect stiffness coefficient $\bar{K}_{ZX}$ is not positive for the whole range of angular position,which is clearly shown in Fig. 21. The variation of $\bar{K}_{zz}$ against angular position of Ist groove of two axial groove bearing is shown in Fig. 22. It is seen that $\bar{K}_{ZZ}$ reduces up to α_{1g} = 90^0 then increasing behavior is seen up to α_{1g} = 150^0.

4.7. Effect of radial position of the grooves on $\bar{C}_{XX}, \bar{C}_{XZ}, \bar{C}_{ZZ}$

Figs. 23-25 show the behavior of $\bar{C}_{XX}, \bar{C}_{XZ}, \bar{C}_{ZZ}$ with groove radial position. The variation of $\bar{C}_{XX}$ is shown in Fig. 23 against radial position of Ist groove radial position, α_{1g} for two axial groove journal bearing. Direct damping coefficient $\bar{C}_{XX}$ increases with increment in radial position of the Ist groove and then reduces. The best value of $\bar{C}_{XX}$ = 6.167 at α_{1g}= 90^0.

The exact value of indirect damping coefficient $\bar{C}_{XZ}(= \bar{C}_{ZX})$ is not positive for all values of radial position, Fig. 24. The absolute maximum value of $\bar{C}_{XZ} = \bar{C}_{ZX}$ is equal to -2.903 at α_{1g}= 90^0. Similar behavior was seen by $\bar{C}_{ZZ}$ (Fig. 25), as observed in the case of $\bar{C}_{XX}$. The best value of $\bar{C}_{ZZ}$ = 7.129 is at α_{1g}= 90^0.

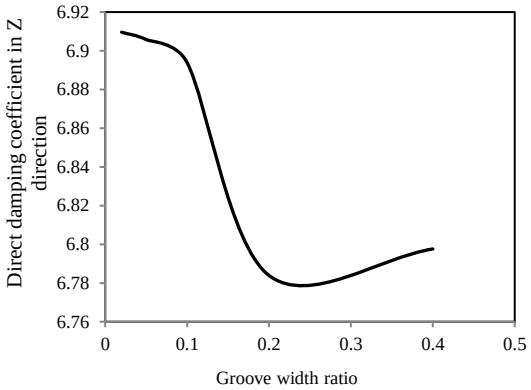

Fig. 18. Effect of w/D on $\bar{C}_{ZZ}$.

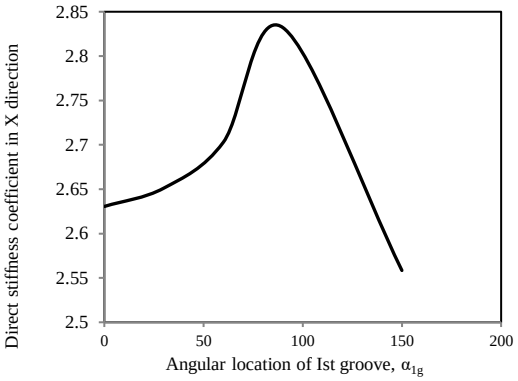

Fig. 19. Effect of radial position of groove on $\bar{K}_{XX}$.

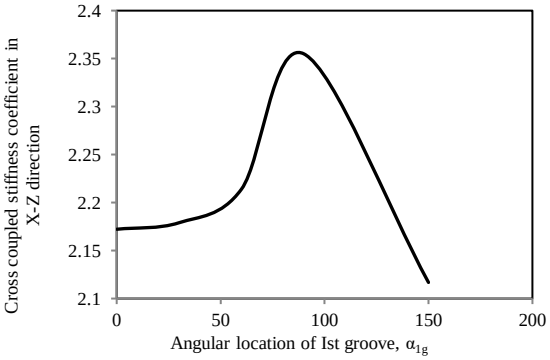

Fig. 20. Effect of radial position of groove on $\bar{K}_{XZ}$.

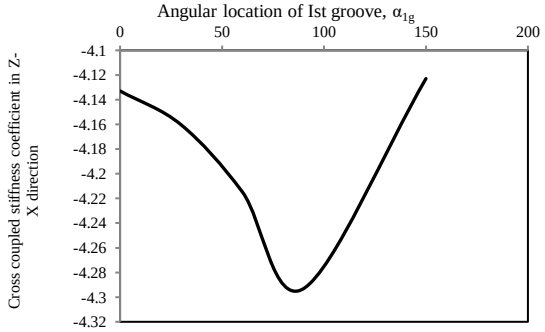

Fig. 21. Effect of radial position of groove on $\bar{K}_{ZX}$.

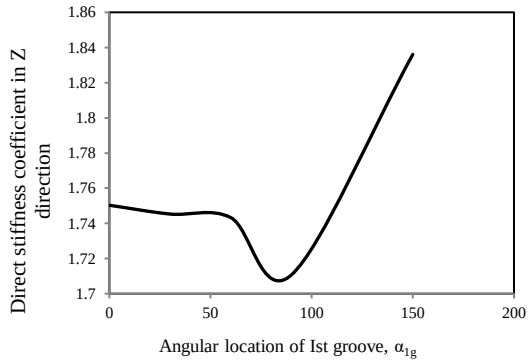

Fig. 22. Effect of radial position of groove on $\bar{K}_{ZZ}$.

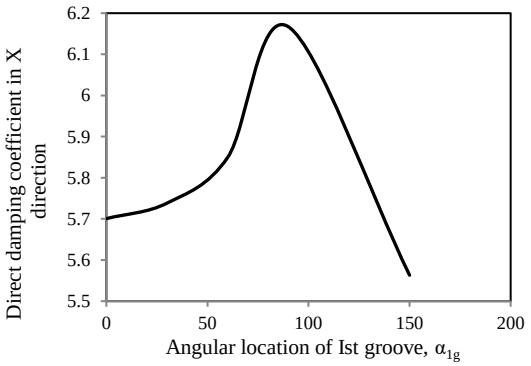

Fig. 23. Effect of radial position of groove on $\bar{C}_{XX}$.

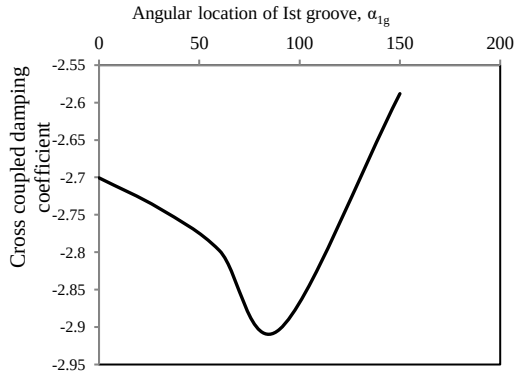

Fig. 24. Effect of radial position of groove on $\bar{C}_{XZ}$

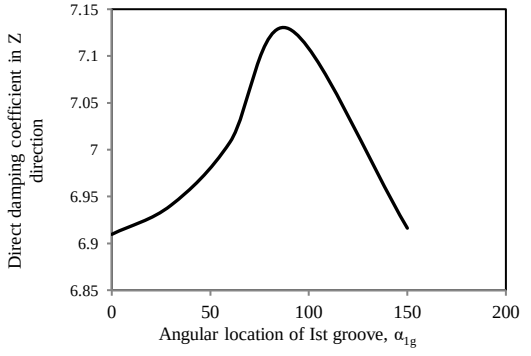

Fig. 25. Effect of radial position of groove on $\bar{C}_{ZZ}$.

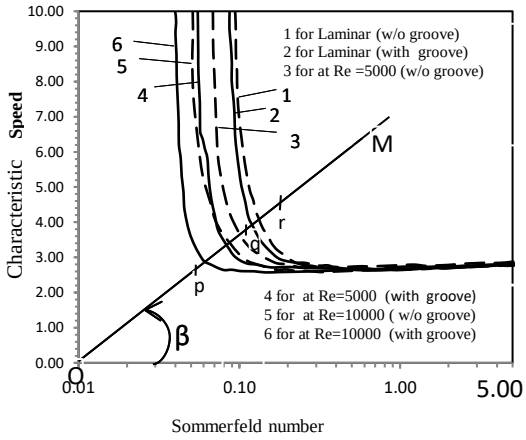

Fig. 26. Comparison chart of characteristic speed for with groove and without groove journal bearing.

5. Stability analysis

Fig. 26 shows the stability chart for the analysis of linearized stability under non-laminar and laminar fluid flow conditions of the two axial groove journal bearing. Fig. 26 plotted between characteristic speed and Sommerfeld number for non-laminar and laminar fluid flow conditions.
The value of the aspect ratio was takes as 0.5 by the author in this study. The obtained trend shows the decrement in characteristic speed for different flow regimes increment in Sommerfeld number and becomes independent of Sommerfeld number for high Sommerfeld number for all flow conditions.
The validation of linearized analysis stability results was drawn for laminar and superlaminar flow conditions along β-line 'OM' shown in Fig. 26. Value of Sn (Sommerfeld number) for different points (p, q, r) on the OM line are given in Table 1. At the fixed velocity of operation with disturbance in displacement $\Delta X_j = \Delta Z_j = 0.005$, the path of the bearing shaft center is shown in Figs. 27 and 28. In this study, no velocity disturbance was taken (i.e. $\Delta \dot{X}_j = \Delta \dot{Z}_j = 0$). In this study, three operating points 'p', 'q', and 'r' were taken for three different flow regimes. The baring shaft (journal) is stable at the point 'p' for all flow regimes (i.e., laminar and turbulent both), as shown in Figs. 27 and 28. It is clearly seen from Fig. 29 that the shaft is stable at the point 'q' in laminar region, but it becomes unstable under turbulence flow condition, Fig. 30. Whereas it is clearly observed

that at point 'r' the journal is always unstable in all flow regimes (i.e. laminar and turbulent regimes, Figs. 31 and 32.)

Table 1. Value of Sn (Sommerfeld number) for different points (p, q, r) on the OM line of Fig. 26.

Operating point	p	q	r
Sommerfeld No.	0.053	0.11	0.17

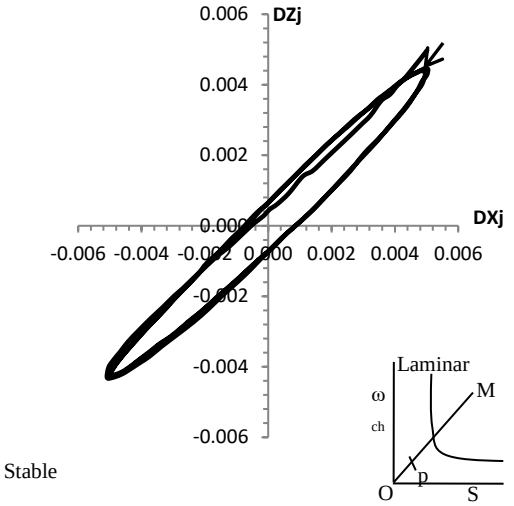

Fig. 27. Path of bearing shaft center with Nonlinearity with fixed velocity along OM line (Laminar flow, L/D = 0.5, Sn = 0.053, at point 'p').

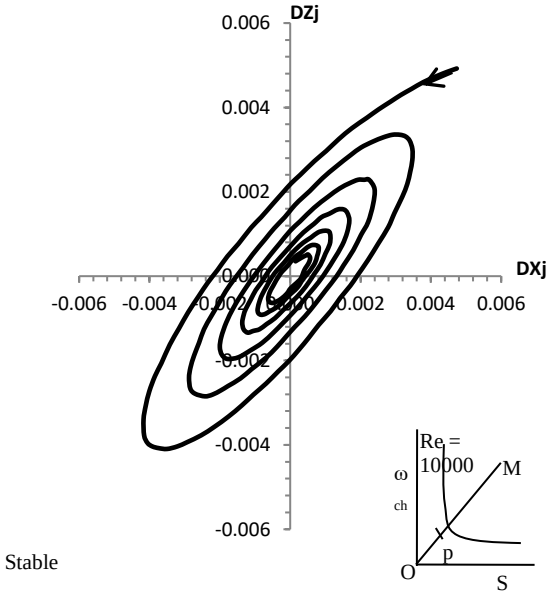

Fig. 28. Path of bearing shaft center with Nonlinearity with fixed velocity along OM line (Re= 10000, L/D = 0.5, Sn= 0.053, at point 'p').

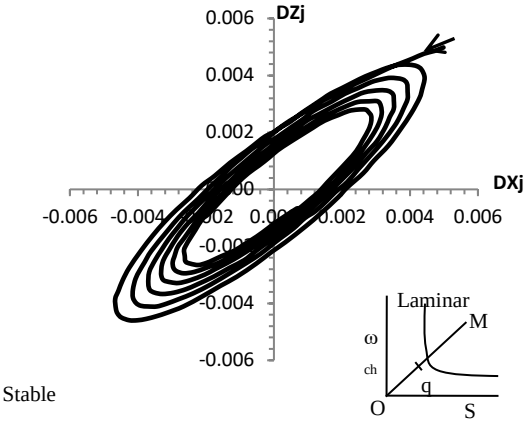

Fig. 29. Path of bearing shaft center with Nonlinearity with fixed velocity along OM line (Laminar flow, L/D = 0.5, Sn =0.11, at point 'q').

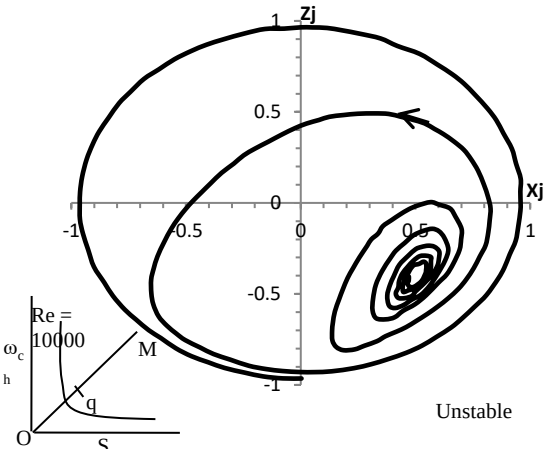

Fig. 30. Path of bearing shaft center with Nonlinearity with fixed velocity along OM line (Re=10000, L/D = 0.5, S_n = 0.11, at point 'q'.

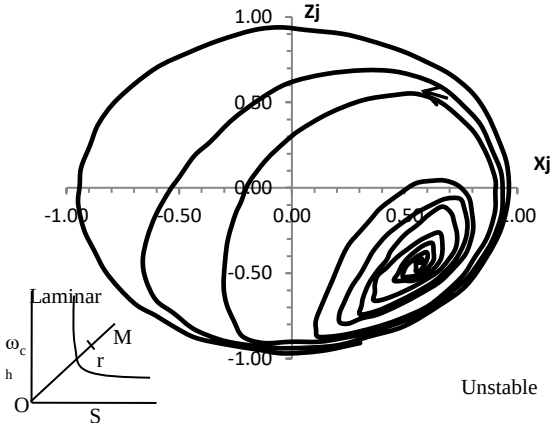

Fig. 31. Path of bearing shaft center with Nonlinearity with fixed velocity along OM line, (Laminar flow, L/D = 0.5, S_n = 0.17, at point 'r').

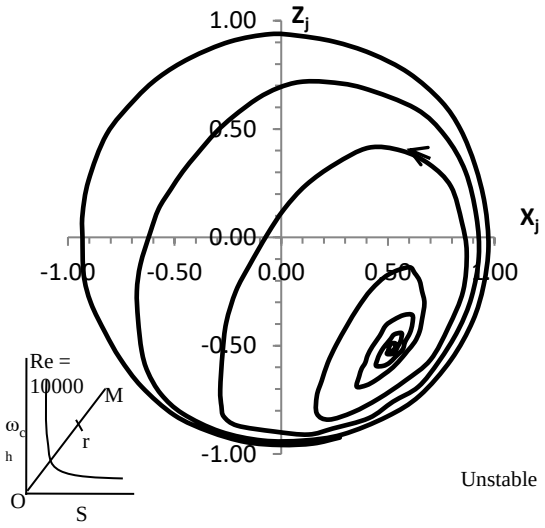

Fig. 32. Path of bearing shaft center with Nonlinearity with fixed velocity along OM line, (Re = 10000, L/D = 0.5, S_n = 0.17, at point 'r').

6. Conclusions

A parametric study of lubricant supply conditions on the performance of non recessed hybrid journal bearings was carried out using the analytical model. Basis on the proposed analytical analysis, the following conclusions are drawn:

1. Non-dimensional load capacity increases with an increase in a/L(a/L), whereas it decreases with an increase in w/D(w/D). The optimum dimension of groove for better static and dynamic characteristic of bearing was obtained as a/L = 0.8, w/D = 0.02, and Ist groove angle α_{1g} = 0^0 (90^0 from load line).
2. The location of the grooves with respect to the load line was found to affect strongly most performance parameters due to the strong interference of the grooves in the hydrodynamic pressure field. The optimum position was found between 60° and 90° (α_{1g} = 0^0) to the load line.
3. The stability of two grooved hybrid bearing reduces due to turbulence. The stability margin reduced with increasing Reynolds number, whereas stability charts shifted towards the left side with increasing Reynolds number.

References

[1] J. P. O'Donoghue, and W. B. Rowe, "Hydrostatic journal bearings (Exact Procedure)", *Tribol. Int.*, Vol. 1, No. 4, pp. 230-236, (1968).

[2] J. P. O' Donoghue, and W. B. Rowe, "Hydrostatic journal design, *Tribol. Int.*, Vol. 2, No. 1, pp.25-71, (1969).

[3] D. Koshal, and W. B. Rowe,"Fluid film journal bearings operating in hybrid mode: Part 1- Theoretical analysis and design", *J. Tribol.*, Vol. 103, No. 4, pp. 558-565, (1981).

[4] D. Koshal, and W. B. Rowe,"Fluid film journal bearings operating in hybrid mode: Part II- Experimental investigation", *J. Tribol.*, Vol. 103, No. 4, pp. 566-572, (1981).

[5] L. San Andres, and A. Z. Szeri, Flow between eccentric rotating cylinders, *ASME J. Appl. Mechs.*, Vol. 51, No. 4, pp. 869-878, (1984).

[6] M. H. Morton, P. G. Johnson, and J. H. Walton, "The influence of grooves in bearing on the stability and response of rotating systems", *Tribol. Ser.*,Vol. 11, No. 1, 347–354, (1987).

[7] M. K. Gethin, D. T. and Delhi El, "Effect of loading direction on the performance of a twin axial groove cylindrical bore bearing, *Tribol. Int.*,Vol. 20, No. 4, pp. 179–185, (1987).

[8] R. Sinhasanand H. N. Chantrawat, "An elastohydrodynamic study on two-axial-groove journal bearing", *Tribol. Int.*, Vol. 21, No. 6, pp. 341-351, (1988).

[9] R. Pai, and B. C. Mazumdar, "Stability of submerged oil journal bearings under dynamic load", *Wear*, Vol. 146, No. 1, pp. 125-135, (1991).

[10] J. M. McCormick and M.G. Salvadori, M.G., *Numerical methods in FORTRAN*, Prentice Hall of India, (1992).

[11] J. C. P. Claro, and A. A. S. Miranda, "Analysis of hydrodynamic journal bearings considering lubricant supply condition", *Proc. Inst. Mech. Eng. Part C: J. Mech. Eng. Sci.*, Vol. 207, No. 1, pp. 93-101, (1993).

[12] A. Kumar, and S. S. Mishra, "Stability of a rigid rotor in turbulent hydrodynamic worn journal bearings", *Wear*, Vol. 193, No. 1, pp.25-30, (1996).

[13] A. Kumar, and S. S. Mishra, "Steady state analysis of noncircular worn journal bearings in non-laminar lubrication regimes", *Tribol. Int*., Vol.29, No. 6, pp.493-498, (1996).

[14] F. A. Martin, "Oil flow in plain steadily loaded journal bearings: Realistic predictions using rapid techniques, *Proc. Inst. Mech. Eng. Part J, J. Eng. Tribol.*, Vol. 212, No. 6, pp. 413–425, (1998).

[15] S. K. KaKoty, and B. C. Mazumdar, "Effect of fluid inertia on stability of journal bearings", *ASME J. Tribol.*, Vol. 122, No.4, pp. 741-745, (2000).

[16] C. T. Jerry, and K. N. Su Lie, "Rotation effects on hybrid hydrostatic /hydrodynamic journal bearings". *Ind. Lub. Tribol.*,Vol. 53, No.6, pp. 261 – 269, (2001).

[17] L. Costa, A.S. Miranda, M. Fillon, J.C.P. Claro, "An analysis of the Effect of oil supply conditions on the thermohydrodynamic performance of a single-groove journal bearing", *Proc. Inst. Mech. Eng. Part J, J. Eng. Tribol.*,Vol. 217, No. 2, pp. 133–144, (2003).

[18] B. C. Majumdar, R. Pai, and D. J. Hargreaves, "Analysis of water lubricated journal bearings with multiple and axial grooves", *Proc. Inst. Mech. Eng. Part J: J. Eng. Tribol.*, Vol. 218, No. 2, pp.135-146, (2004).

[19] C. Desai, D. Patel, "Experimental analysis of pressure distribution of Hydrodynamic Journal Bearing: A parametric study", *Proc. Int. Conf. Mech. Eng.*, pp.1-4, (2005)

[20] F. P. Brito, J. Bouyer, M. Fillon and A. S. Miranda, "Thermal behavior and performance characteristics of a twin axial groove journal bearing as a function of applied load and oil supply temperature", TRIBOLOGIA Finnish, *J. Trib*., Vol. 3, No.1, pp.24–33, (2006).

[21] F. P. Brito, A. S. Miranda, J. Bouyer, M. Fillon, "Experimental Investigation of the Effect of Supply Temperature and Supply Pressure on the Performance of a Two-Axial Groove Hydrodynamic Journal Bearing", *J. Tribol.*, Vol. 129, No. 1, pp. 98, (2007).

[22] L. Roy, and S. K. Laha, "Steady state and dynamic characteristics of axial grooved journal bearings", *Tribol. Int.*, Vol. 42, No. 5, pp. 754-761, (2009).

[23] R. R. Navthar, and N. V. Halegowda, "Stability Analysis of Hydrodynamic Journal Bearing using Stiffness", *Int. J. Eng. Sci. Tech.*, Vol. 2, No. 2, pp.87–93, (2010).

[24] N. P. Mehta, S.S. Rattan, and R. Verma, "Stability analysis of two lobe hydrodynamic journal bearing with couple stress lubricant", *ARPN J. Eng. Appl. Sci*., Vol. 5, No. 1, pp.69-74, (2010).

[25] M. V. Kini, R. S. Pai, D. S. Rao, S.B. Satish, R. Pai, "Effect of groove location on the dynamic characteristics of multiple axial groove water lubricated journal bearing", *World Acad. Sci. Eng. Technol.*, Vol. 60, pp. 1592–1596, (2011).

[26] F.P. Brito, A.S. Miranda, J.C.P. Claro, M. Fillon, "Experimental comparison of the performance of a journal bearing with a single and a twin axial groove configuration", *Tribol. Int.*, Vol. 54, No.1, pp.1–8, (2012).

[27] L. Roy, S.K. Kakoty, "Optimum groove location of hydrodynamic journal bearing using genetic algorithm", *Adv. Tribol.*, Vol. 2013. No. 1, pp. 1-13 (2013).

[28] V. K. Dwivedi,S. Chand , K. N.Pandey, "Effect of Number and Size of Recess on the Performance of Hybrid (Hydrostatic/Hydrodynamic) Journal Bearing", *Proc. Eng.*, Vol. 51, pp. 810-817, (2013).

[29] V. K. Dwivedi,S. Chand , K. N.Pandey, "Effect of Different Flow Regime on the Static and Dynamic Performance Parameter of Hydrodynamic Journal Bearing", *Proc. Eng.*, Vol. 51, pp. 520-528, (2013).

[30] V. K. Dwivedi,S. Chand , K. N.Pandey, "Effects of turbulence on dynamic performance of accelerated / decelerated hydrodynamic journal bearing system", *Int. J. Des. Eng*., Vol. 5 No. 3, pp. 256–288, (2014).

[31] F. P. Brito, A.S.Miranda, J.C.P. Claro, J. C. Teixeira, L. Costa, and M. Fillon, "Thermohydrodynamic modeling of

journal bearings under varying load angle and negative groove flow rate", *Proc. Ist. Mech. Eng. Part J: J. Eng. Tribol.*, Vol. 228, No. 9, pp. 955-973, (2014).

[32] V. K. Dwivedi,S. Chand , K. N.Pandey, "Stability Analysis of Twin Axial Groove Hybrid Journal Bearing", *J. Appl. Fluid Mechs.*, Vol. 9, No. 6, pp. 2763-2768, (2016).

[33] S. Sharma, R. K. Awasthi, "Performance of hydrodynamic journal bearing operating under transient wear", *Mechs. Mech. Eng.*, Vol. 22, No. 1, pp. 153-170, (2018).

[34] J. Wang, J. Zhang, J. Lin and L. Ma. "Study on lubrication performance of journal bearing with multiple texturedistributions", *Appl. Sci.*, Vol. 8, No. 2, pp. 244-256, (2018).

[35] V. N. Constantinescu, 'The pressure equation for turbulent lubrication', Proc. Conf. on Lubrication and Wear, *Proc. Inst. Mech. Eng.*, Vol. 182, No. 3A, pp.383–400, (1967).

How to cite this paper:

Vijay Kumar Dwivedi, Pooja Pathak, "Effect of axial groove location, length and width ratio on bearing properties and stability, *J. Comput. Appl. Res. Mech. Eng.*, Vol. 10, No. 2, pp. 525-537, (2021).

DOI: 10.22061/jcarme.2019.4411.1541

URL: https://jcarme.sru.ac.ir/?_action=showPDF&article=1071